Batteries & Supercaps

Research Article
doi.org/10.1002/batt.202400735

Chemistry Europe
European Chemical Societies Publishing

www.batteries-supercaps.org

Dynamic Mechanism of Short Peptide Additive Regulating Solvation Microenvironment of Zinc Ions

Yuting Li,[a] Danyang Xiong,[a] Jiabao Zhu,[a] Yulan Mou,[a] Jinrong Yang,*[a] and Xiao He*[a, b, c]

The optimization electrolyte strategy through molecular additives to improve the stability of aqueous zinc-ion batteries (AZIBs), which changes the solvation structure of hydrated zinc ions (Zn^{2+}), generally relies on experimental trial and error, because the precise mechanism by which these additives alter the coordination environment of Zn^{2+} remains elusive. Here, we select the oligopeptide of mono-, di-, tri-, and tetra-glycine, as electrolyte additives to optimize the Zn^{2+} solvation microenvironment in AZIBs. Contrary to traditional views, we find that these additives modify the solvated structure of the Zn^{2+} by substituting sulfate ion (SO_4^{2-}) in the preexistence of Zn^{2+}-SO_4^{2-} ion pair, rather than water molecules in the first solvation shell, due to a high energy barrier to replace one of the coordinated water molecules of Zn^{2+}. This observation is consistent with recent experimental result of the attenuating influence of glycine on the interaction between Zn^{2+} and SO_4^{2-} confirmed by Fourier-transform infrared spectroscopy. For the multifunctional triglycine, its favorable conformation is disrupted to accommodate the direct coordination of oxygen atoms with Zn^{2+}, and Zn^{2+} is observed to migrate between distinct sites along the triglycine backbone. This work provides theoretical principles to rationally design advanced electrolytes for solvation modulation with high performance AZIBs.

Introduction

Aqueous zinc-ion batteries (AZIBs) have garnered substantial research because of their high theoretical capacity (820 mAh g^{-1}), low redox potential (−0.76 V vs standard hydrogen electrode), simple preparation process and high safety.[1–3] Despite these advantages, the cycling process of the zinc anode is fraught with the non-uniform electric field distribution, which leads to uneven nucleation of zinc ions (Zn^{2+}) associated with the growth of dendrites.[4] Additionally, the side reactions such as hydrogen evolution reaction (HER), corrosion, and passivation[5,6] are exacerbated, resulting in a significant deterioration in the performance and cycle life of zinc electrodes. To address these issues, numerous strategies have been proposed, such as surface modification,[7,8] the construction of artificial interfacial layer,[8] the design of Zn anode structure,[9] the optimization of diaphragm design,[10] constructing solid electrolyte interphase (SEI),[11] introducing hydrogen bonds to improve organic electrode materials,[12] selecting Aqueous Hydrogen Proton Batteries (AHPB)[13] and the use of electrolyte additives.[14] Among these, the use of electrolyte additive stands out as a favored strategy because of its simplicity and low cost.

Current studies highlight significant improvements in battery performance through electrolyte additives, broadly categorized as inorganic and organic. The inorganic additives encompass Na_2SO_4,[15] $Ni(TfO)_2$,[16] $ZnBr_2$,[17] LiF, SnO, K_2CO_3,[18–20] among others. For example, Kim et al.[21] utilized the hardness of the Sc^{3+} additive hydration shell to effectively avoid the accumulation of Zn^{2+} at the tips of zinc metal surface, thereby inhibiting dendrite growth. Similarly, Zhu et al.[22] introduced a highly concentrated supporting salt, $NaClO_4$, into the electrolyte. This dominated the cationic solvation shell, suppressed water activity, and resulted in >99% Coulombic efficiency (CE) with exceptional cycling stability. The organic additives includes polyacrylamide (PAM),[23] cetyltrimethylammonium bromide (CTAB),[24] carboxymethyl cellulose (CMC),[25] and silk fibroin (SF),[26] etc. Jiao et al.[27] employed trisodium nitrilotriacetate (Na_3NTA) as an additive to replace the water molecules in the solvated structure of Zn^{2+}, effectively inhibiting the side reactions and the lifetime of Zn||Zn symmetric batteries using the modified electrolyte can reach 3000 h at a cut-off capacity of 1 mA h cm^{-2}. In addition, Hou et al.[28] used urea to modulate the solvation structure of Zn^{2+} – $[Zn(H_2O)_2(NH_3)_3]^{2+}$, suppressing dendrites and preventing "dead zinc," achieving a Zn/birnessite full cell energy density of 280 Wh kg^{-1} and a service life of 5000 cycles. These collective findings underscore the pivotal role of electrolyte additives in advancing the performance and longevity of AZIBs, offering a strategic approach to address the challenge related to battery stability.

Building on these advancements in AZIBs, glycine has emerged as a promising organic additive that addresses several limitations inherent to conventional organic additives. Unlike many organic compounds that are characterized by high toxicity, high cost-effectiveness, and limited functionality,

[a] Y. Li, D. Xiong, J. Zhu, Y. Mou, J. Yang, X. He
Shanghai Engineering Research Center of Molecular Therapeutics and New Drug Development, Shanghai Frontiers Science Center of Molecule Intelligent Syntheses, School of Chemistry and Molecular Engineering, East China Normal University, Shanghai 200062, China
E-mail: jryang@chem.ecnu.edu.cn
xiaohe@phy.ecnu.edu.cn

[b] X. He
Chongqing Key Laboratory of Precision Optics, Chongqing Institute of East China Normal University, Chongqing 401120, China

[c] X. He
New York University-East China Normal University Center for Computational Chemistry, New York University Shanghai, Shanghai 200062, China

Supporting information for this article is available on the WWW under https://doi.org/10.1002/batt.202400735

Research Article
doi.org/10.1002/batt.202400735
Chemistry Europe
European Chemical Societies Publishing

glycine offers a biodegradable and environmentally friendly alternative.[29] For instance, Lin et al.[30] revealed the superior cycle reversibility of 7000 hours in zinc symmetric batteries with $ZnSO_4$-Glycine electrolyte. Similarly, Luo et al.[31] reported an average CE of 99.22% at 1 mA cm^{-2} and 0.5 mAh cm^{-2} for AZIBs over 500 cycles when glycine was used as an additive. However, in experimental studies, the effects of additives on solvation structures are often inferred by a suite of analytical techniques, including Raman spectroscopy, Fourier transform infrared spectroscopy (FTIR), and nuclear magnetic resonance (NMR) spectral shifts. For example, in the study by Yu et al.,[32] Raman and FT-IR spectroscopy showed that the peak of the v-SO_4^{2-} band shifted to a lower frequency, the proportion of contact ion pairs (CIP) gradually decreased, and the stretching vibration of v-SO_4^{2-} exhibited a blue shift after the addition of glycine. These findings demonstrate that glycine molecules can easily enter the CIP structure and replace one of the original SO_4^{2-} groups. Concurrently, theoretical computational studies employ fundamental dynamic simulation methodologies, complemented by radial distribution function (RDF) and coordination number (CN) analyses, to substantiate these experimental inferences. According to the simulation results of RDF and CN, Zhang et al.[33] inferred the formation of a new solvation structure with the average coordination number of Zn^{2+}-O(H_2O) 5.98 reduced to 5.2 after the addition of the triglycine. Despite these approaches, a comprehensive understanding of the underlying dynamic mechanisms at the molecular level remains an area ripe for further exploration.

Herein, we delve into the dynamic mechanisms by which additives optimize the solvation structure of Zn^{2+} at the atomic level. To achieve this, we have selected oligopeptide of mono-, di-, tri- and tetra-glycine as molecular additives and introduced them into $ZnSO_4$ solutions of varying concentrations (0.1, 1, and 2 M) for classical molecular dynamics simulation. The metadynamics simulation results indicate that replacing water molecules in the primary solvation sheath of Zn^{2+} by additive molecules entails overcoming a significant energy barrier. This finding elucidates the anomalous phenomenon that additive molecules optimize the solvation structure of Zn^{2+} through the mediation of sulfate ions. The energy barrier differences in the desolvation process of Zn^{2+} before and after the introduction of the additive corroborates previous reports that glycine molecules can enhance the stability of Zn^{2+} deposition/stripping by reducing the desolvation energy barrier. This work provides a theoretical framework for understanding how oligopeptide additives optimize the solvation structure of Zn^{2+}, offering guidance for the development of advanced electrolyte systems aimed at improving the performance of AZIBs.

Methods

System Building

To simulate the individual systems, multiple periodic water boxes with dimensions of 5×5×5 nm^3 are constructed. Based on the pre-calculated quantities of additives and ions (Table 1), the corresponding solutes are inserted into the system using the software's built-in water molecule replacement function.

Table 1. Composition of additive solutions with varying concentrations of $ZnSO_4$.

Solution	Additive (count)	Cations (count)	Anions (count)	Waters (count)	Box length (nm)
Pure 0.1 M $ZnSO_4$	0	8	8	4023	5
Pure 1 M $ZnSO_4$	0	70	70	3748	5
Pure 2 M $ZnSO_4$	0	140	140	3400	5
Pure 3 M $ZnSO_4$	0	280	280	3130	5
0.1 M $ZnSO_4$ +0.1 M G*	7	8	8	3988	5
1 M $ZnSO_4$ +0.1 M G	7	70	70	3714	5
2 M $ZnSO_4$ +0.1 M G	7	140	140	3423	5
0.1 M $ZnSO_4$ +0.1 M GG*	7	7	7	3971	5
1 M $ZnSO_4$ +0.1 M GG	7	70	70	3695	5
2 M $ZnSO_4$ +0.1 M GG	7	140	140	3392	5
0.1 M $ZnSO_4$ +0.1 M GGG*	7	7	7	3953	5
1 M $ZnSO_4$ +0.1 M GGG	7	70	70	3669	5
2 M $ZnSO_4$ +0.1 M GGG	70	70	140	3372	5
0.1 M $ZnSO_4$ +0.1 M GGGG*	7	7	7	3953	5
1 M $ZnSO_4$ +0.1 M GGGG	7	70	70	3669	5
2 M $ZnSO_4$ +0.1 M GGGG	70	70	140	3372	5

*G stands for glycine, GG stands for diglycine, GGG stands for triglycine, GGGG stands for tetraglycine.

Molecular Dynamics Simulations

All simulations were carried out within the GROMACS software package (version 2023).[34] During the molecular dynamics equilibrium process, firstly, the system's energy is minimized using the Steepest Descent algorithm. This is followed by a 500 ps NPT simulation to ensure temperature stability, after which a 100 ns production simulation is conducted. The force fields for the additives (glycine, diglycine, triglycine, tetraglycine) are based on the Generalized Amber Force Field (GAFF) generated by the Sobtop[35] program. The force field for Zn^{2+} (amber03.ff) is included with GROMACS, while the force field for SO_4^{2-} is referenced from Williams et al..[36] The SPC/E model is used to describe the water molecules.[37] Subsequent calculations of conductivity, structural analysis, and interaction energy are performed based on the results of the production simulation data.

Metadynamics simulation (metaD) was used to calculate the potential of mean force (PMF), which is implemented by interfacing GROMACS with the PLUMED library.[38–40] The distance between the Zn^{2+} and all oxygen atoms in the additive is set as collective variables (CVs), with Gaussian deposited every 500 steps. The initial height of the Gaussian is set to 0.2 kJ/mol with width of 0.2 Å and

Research Article
doi.org/10.1002/batt.202400735
Chemistry Europe
European Chemical Societies Publishing

bias factor of 20. To focus on the behavior of additive molecules around the solvation sheath of Zn^{2+}, we impose an upper wall potential with a bounding value set to 6 Å, sampling is performed for 100 ns at a step size of 2 fs. The LINCS scheme[41] is used to fix the bond distances involving H atoms. The V-rescale[42] thermostat is used for temperature control of 300 K, while the pressure is controlled at 1 bar using an isotropic C-rescale barostat. The cutoff distance for non-bonded interactions is set to 12 Å, and the PME method is employed to handle long-range Coulomb interactions.

DFT Calculations

The binding energies of additive (Add), Zn^{2+} and H_2O are calculated by Gaussian16[43] software, defined as:

$$\Delta E_{binding} = E_{[Zn^{2+}-Add/H_2O]} - E_{Add/H_2O} - E_{Zn^{2+}} \quad (1)$$

where $E_{[Zn^{2+}-Add/H_2O]}$ is the total energy of Zn^{2+} and water or additives, E_{Add/H_2O} is the total energy of water or additives, $E_{Zn^{2+}}$ is the total energy of Zn^{2+}, $\Delta E_{binding}$ is the binding energy of water or additives with Zn^{2+}. Additionally, the desolvation energy between the $[Zn^{2+}\text{-}(H_2O)_n]$ and $[Add\text{-}Zn^{2+}(H_2O)_{n-1}]$ is calculated by this formula:

$$\Delta E = E_{[Zn^{2+}-(H_2O)_n]} - E_{[Zn^{2+}-(H_2O)_{n-1}]} - E_{H_2O} \quad (2)$$

$$\Delta E = E_{[Add-Zn^{2+}-(H_2O)_n]} - E_{[Add-Zn^{2+}-(H_2O)_{n-1}]} - E_{H_2O} \quad (3)$$

where $E_{[Zn^{2+}-(H_2O)_n]}$ is the total energy between the Zn^{2+} and n water molecules, $E_{[Zn^{2+}-(H_2O)_{n-1}]}$ is the total energy of Zn^{2+} and n-1 water molecules, $E_{[Add-Zn^{2+}-(H_2O)_n]}$ is the total energy between Zn^{2+}, water and additives, E_{H_2O} is the total energy of Zn^{2+}, ΔE is the energy required to remove a water molecule.

The free energy changes (4) for the dehydration process of replacing a water molecule in the 1st solvation sheath of Zn^{2+} with additive, as well as the solvation energies (5) for the removal of a water molecule, are described by the following equation:

$$Zn^{2+} - (H_2O)_n + Add \rightarrow Add - Zn^{2+} - (H_2O)_{n-1} + H_2O \quad (4)$$

$$Zn^{2+} - (H_2O)_n \rightarrow Zn^{2+}(H_2O)_{n-1} + H_2O \quad (5)$$

where n represents the number of water molecules in the initial structures. All calculations are performed at the M06-2X/6-311+G(d, p) level for structure optimization and frequency calculations, with zero-point energy corrections applied to all results.

Conductivity Calculations

The calculation of electric conductivity(σ) is based on Green-Kubo's formula[44]

$$\sigma = \frac{1}{3k_B TV}\int_0^\infty dt\,(J(t)\cdot J(0)) \quad (6)$$

with an equilibrated MD to obtain the associated time-dependent function, where k_B is the Boltzmann constant, T is the system temperature, V is the system volume, t is time, and J is the charge current defined as

$$J(t) = \sum_i q_i v_i(t) \quad (7)$$

with q_i and v_i being the charge and the velocity of the ion particle, respectively.

Radial Distribution Function (RDF) and Coordination Number (CN) Calculations

The RDF[45] shows the probability of finding another ion at a distance r from a reference ion. The RDF is calculated as follows:

$$g(r) = \frac{V}{N^2}\left(\sum_i \sum_{j\neq i} \delta(r - r_{ij})\right) \quad (8)$$

where V represents the system volume and N is the number of ions in the system. The CN indicates the number of nearest neighboring ions around an ion, which can be calculated by the following formula:

$$CN_{\alpha\beta} = \int_0^{r_{cut}} 4\pi r^2 \rho_\beta g_{\alpha\beta}(r)\,dr \quad (9)$$

where r_{cut} is a minimum after the first peak of the RDF and ρ_β is the average number density of ions of type β in the system.

Results and Discussion

The comprehensive modification mechanism of the molecular additive, as illustrated in Figure 1, elucidates the transition from an additive-deficient scenario to one enriched with glycine. In the absence of an efficacious additive, water molecules, particularly those within the solvation sheath of Zn^{2+} ions, exhibit heightened activity and are susceptible to reduction, leading to the hydrogen evolution reaction (HER) and consequently, the growth of metal dendrites. The introduction of glycine as an additive prompts a significant shift, wherein glycine molecules replace H_2O in the solvation structure surrounding Zn^{2+} through the mediation of sulfate ions. This

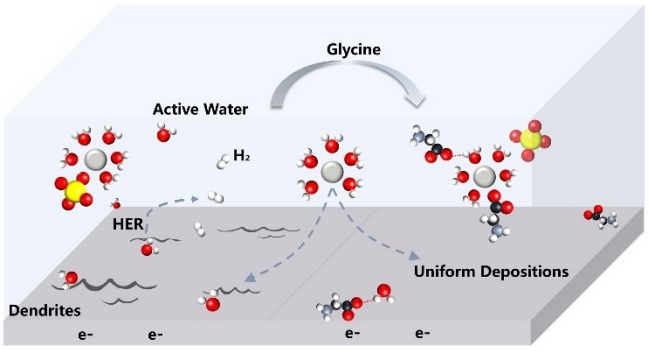

Figure 1. Left: Issues of zinc anode – dendrite growth and side reactions. Right: Glycine additive modifies the Zn^{2+} solvation structure by replacing sulfate ion and forming hydrogen bonds with water, inhibiting HER and dendrite growth.

Research Article
doi.org/10.1002/batt.202400735
Chemistry Europe
European Chemical Societies Publishing

substitution restructures the hydrogen-bond networks within the diffusion layer and enables glycine to preferentially adsorb and undergo reduction at the anode. These alterations diminish the activity of H_2O, effectively curbing the HER and fostering even Zn metal deposition.

Structural Analysis

In order to determine the coordination sites of the molecular additives of glycine (G), diglycine (GG), triglycine (GGG), and metal ions, we calculate the electrostatic potential surfaces (ESPs) (shown in Figure 2a) using the Multiwfn[46] and VMD[47] software packages. The results show that the negative charges of G are mainly concentrated on the carboxyl group acting as an electron donor, which implies that the electrostatic attraction between Zn^{2+} and additive molecules is strong.[48] These negatively charged groups can act as nucleophilic sites to cooperate with Zn^{2+}, which can regulate the solvation structure of Zn^{2+} and guide the nucleation and deposition of Zn^{2+}.[31] Next, we construct several molecular dynamics (MD) simulation systems (Figure 2b) by introducing G, GG, and GGG as additives, respectively, to investigate the effect of additive chain lengths on the structure of the ionic solvation under different concentrations of zinc salts.

To quantitatively assess the solvation sheath of Zn^{2+}, we calculate the RDF [g(r)] for the oxygen atoms coordinated with Zn^{2+}, specifically Zn^{2+}-O(H_2O) and Zn^{2+}-O(additive), along with the CN [n(r)] (Figure 2c–f). In the pure $ZnSO_4$ solution (Figure 2c), the RDF profile exhibits a distinct peak at 2 Å, indicating a strong interaction between Zn^{2+} and water molecules in the first hydration sheath. The boundary of this sheath is observed at approximately 3.5 Å with n(r) of 5.8, suggesting that the first hydration sheath of Zn^{2+} comprises six water molecules to form the $[Zn(H_2O)_6]^{2+}$ complex, consistent with result of Chen et al..[49] Additionally, g(r) displays another peak around 4.2 Å, indicative of the second hydration sheath, with its boundary located at approximately 5.3 Å. As the concentration of Zn^{2+} increases from 0.1–2 M, the RDF curves exhibit an enhancement in the Zn^{2+}-O(H_2O) peak at 2 Å, indicating that the interaction between water molecules and Zn^{2+} becomes stronger, consistent with the experimental study of Yu et al..[50] The n(r) profile reveals a decrease in the number of water molecules in the first solvation sheath from 6.0–5.6, suggesting a reduction in the proportion of coordinated water molecules as the $ZnSO_4$ electrolyte concentration increases. For comparison, we calculate the CN of Zn^{2+} and water after the addition of the three kinds of additives, as shown in Figure S1. The positions and displayed intensities of the peak are similar to those in the pure $ZnSO_4$ solution. The RDF curves for Zn^{2+}-O(additive) reveal two distinct peaks at approximately 1.9 Å and 4.1 Å (Figure 2d–f), indicating that the additive molecules occupy the first and second solvation sheaths. Additionally, these additive molecules can interact with residual water molecules through hydrogen bonding (Figure S2). Such substitutions and interactions enhance the stability of water molecules, reducing their activity.[51]

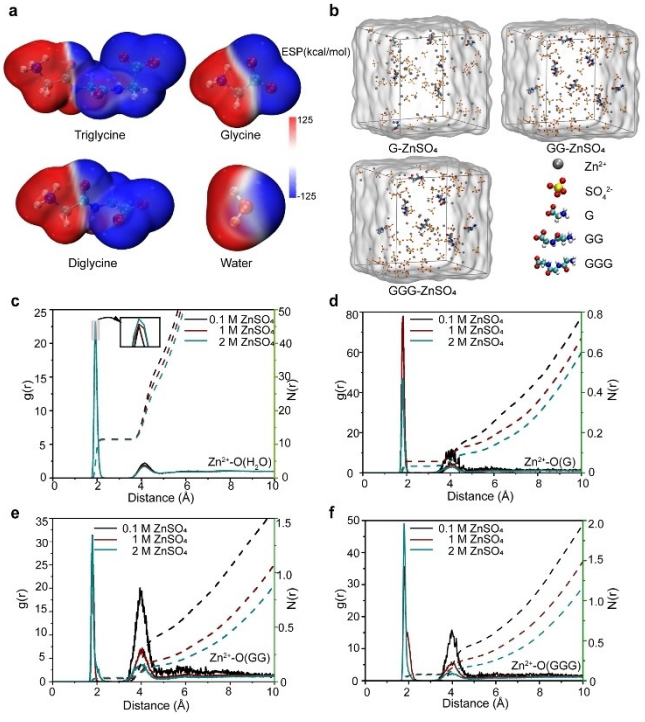

Figure 2. Characterization of solvation structure in $ZnSO_4$-additive electrolyte system. **a)** Electrostatic potential map of the G, GG, GGG. **b)** Simulation box snapshots of G-$ZnSO_4$, GG-$ZnSO_4$, GGG-$ZnSO_4$ systems. **c–f)** Radial distribution function *g*(*r*) and CN *N*(*r*) for: Zn^{2+}-O(H_2O) and Zn^{2+}-O(additive) in 0.1, 1, and 2 M $ZnSO_4$ with 0.1 M additive (G, GG, GGG) aqueous electrolyte.

Microscopic Dynamic Mechanisms

In order to investigate how additive molecules penetrate the first solvation sheath of Zn^{2+}, we obtain the potential of mean force (PMF) profile of different additives carbonyl oxygen atoms (C═O) approaching Zn^{2+} via metaD (Figure 3a). The PMF results show substantial energy barriers of 8.2, 8.7 and 7.3 kcal/mol for the G, GG and GGG, respectively, when displacing a water molecule to enter the first solvation sheath of Zn^{2+}. We observe that as the chain length increases, the energy barrier exhibits a decreasing trend. We have further extended the chain length of the additive by incorporating GGGG and calculated the energy barrier for tuning the solvation shell of Zn^{2+}. The energy barrier is found to be 7.2 kcal/mol (Figure S3), slightly lower than that of GGG. This result further confirms that increasing the chain length of glycine-based additives potentially favors the optimization of the Zn^{2+} solvation shell structure. Notably, the energy barrier for GG to enter the solvation sheath of Zn^{2+} is slightly higher than that for G. The higher energy barrier can be attributed to a combination of molecular flexibility, electrostatic interactions, and solvation effect. (Detailed discussions are in the SI) Additionally, we also consider the effect of additive concentration by setting up concentration gradients of 0.03, 0.10, and 0.20 M. Figure S4 shows that as the concentration of additives increases, the energy barriers for the four additives entering the Zn^{2+} solvation shell decrease. These results indicate that higher additive concentrations positively influence

Research Article
doi.org/10.1002/batt.202400735
Chemistry Europe
European Chemical Societies Publishing

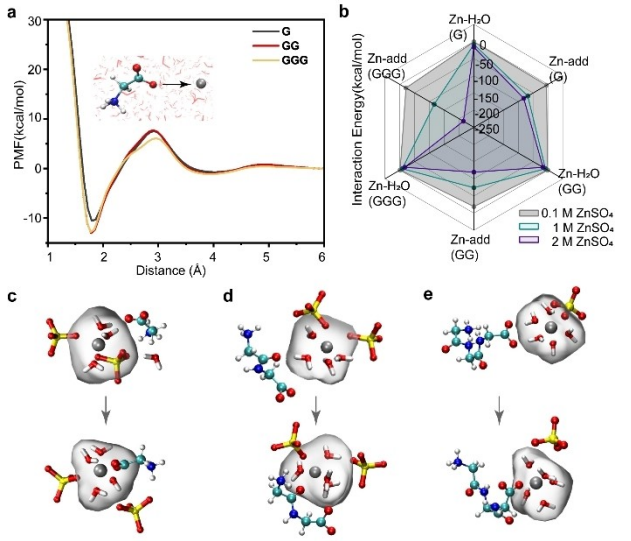

Figure 3. a) The PMF curves for the interaction between additives (G, GG, GGG and GGGG) and Zn^{2+} at 2 M concentration. Black represents G, red for GG, yellow for GGG and blue for GGGG. **b)** Interaction energies between Zn^{2+} and additives (G, GG, GGG) and H_2O at various concentrations. The figure notes are the objects of the interactions, and the labeling in parentheses refers to the additives introduced in the corresponding system. **c–e)** Snapshots of G, GG and GGG displace sulfate into the first solvation sheath of Zn^{2+}.

the modification of the solvation structure of Zn^{2+}, further improving the efficiency of solvation shell modification.

Moreover, once additives successfully coordinate with Zn^{2+}, newly formed solvation structures show good stability. Because they require considerable energy barriers of 18.1, 20.8 and 18.9 kcal/mol, respectively, to detach from the first solvation sheath of Zn^{2+}. And, by quantifying the electrostatic and van der Waals interactions between the additive molecules, water molecules and Zn^{2+} (Figure 3b, the detailed values are given in Table S1), we find that electrostatic forces dominate. The total interaction of additives with Zn^{2+} is much stronger than that between water and Zn^{2+}. For example, for the 1 M $ZnSO_4$-GGG system, the total interaction energy between Zn^{2+} and GGG is −116.0 kcal/mol, while the interaction energy between Zn^{2+} and water is only −8.5 kcal/mol. In addition, the longer the chain of additives is, the more significant the interaction with Zn^{2+} is. For the concentration of $ZnSO_4$ up to 2 M, the interaction of G, GG, GGG with Zn^{2+} are −81.8, −119.3, −214.6 kcal/mol, respectively, showing a significant increase.

According to some experimental results,[33,52] G can enhance battery performance by modifying the solvation structure of Zn^{2+}. Our computational results also show that G and its oligomers (GG, GGG) strongly interact with Zn^{2+}. However, we also find that G must overcome a certain energy barrier to replace a water molecule into the first solvation shell of the Zn^{2+}. We further monitor the dynamic process through MD simulations, and find that G, GG, and GGG all enter the solvation shell by replacing a sulfate ion from the contact ion pair (CIP/$[Zn(H_2O)_x(SO_4)_y]^{2-2y}$,[50] thereby directly coordinating with the Zn^{2+} (Figure 3c–e). This mechanism by which the additive replaces sulfate ions rather than coordinated water provides new insights into how amino acid additives optimize the environment around Zn^{2+}, consistent with the experimental result of Liu et al..[32] They observed through FTIR that the introduction of additives leads to a blue shift in the stretching vibration of SO_4^{2-} and disrupts the electrostatic coupling between Zn^{2+} and SO_4^{2-}, suggesting that G has replaced a sulfate ion. We conduct density functional theory (DFT)-calculated vibrational spectra for [GGG-Zn^{2+}-H_2O], compared to pure $ZnSO_4$ solution system. As shown in Figure S5, the introduction of additives causes a significant blue shift in the stretching vibration of SO_4^{2-}, which is consistent with the experimental observation.

Based on the above analysis of electrolytes, G as an additive can regulate the activity of solvated water molecules through the formation of direct contact state (i.e. direct coordination between the two without solvent molecules in between) with Zn^{2+}. However, further in-depth studies of the microdynamic process of this modulation mechanism are still needed. Notably, conductivity is one of the key parameters for optimizing the electrolyte concentration. Although higher electrolyte concentrations can enhance the regulatory effect of glycine on the solvation structure, excessively high salt concentrations may lead to an increase in solution viscosity, reducing ion mobility and diffusion coefficients (Figure S6), ultimately having a negative impact on conductivity.[53,54] The calculated conductivity of the 2 M $ZnSO_4$ solution is found to be an optimal concentration of 15.0 $S\,m^{-1}$ (as shown in Figure 4a), conforming to the experimental trend.[55] Additionally, we also calculate the conductivity of the $ZnSO_4$ solution in the presence of additives. (Figure S7) The simulation results indicate that the addition of the additives leads to a slight decrease in the ionic conductivity of Zn^{2+}, which may be attributed to the presence of the additives partially hindering the migration and diffusion of Zn^{2+}. However, the overall trend in the conductivity data remains consistent with the system without additives.

Based on the CN calculation in Figure 4b (The detailed values are given in Table S2), the predominant CN of Zn^{2+} with water molecules is 6, consistent with the calculation results of RDF. With the increasing chain length of the additive molecules, the proportion of Zn^{2+} with CN-6 [CN-n represents the coordination number of Zn^{2+}-O(H_2O)] decreases, while the proportion of Zn^{2+} with CN-5 increases. Notably, in the presence of GGG, the proportions of Zn^{2+} with CN-3 and CN-4 also increase, with the corresponding snapshot in the Figure 4c. It is evident that by increasing the active sites of the additive for interaction with metal ions, the additive can displace more coordinated water, allowing for direct chelation with the metal ions.

By calculating the number of oxygen atoms from the GGG residues entering the first solvation sheath of Zn^{2+} in the system, we find that multiple GGG molecules can stably coordinate with the Zn^{2+} with 1–3 oxygen atoms during the entire dynamic process (Figure S8). To delve into the microscopic dynamic regulation mechanism of additive molecules within the Zn^{2+} solvation sheath, we conduct a tracking analysis of the structural changes between Zn^{2+} and different oxygen atoms along the backbone of GGG throughout the entire

Research Article
doi.org/10.1002/batt.202400735

Chemistry Europe
European Chemical Societies Publishing

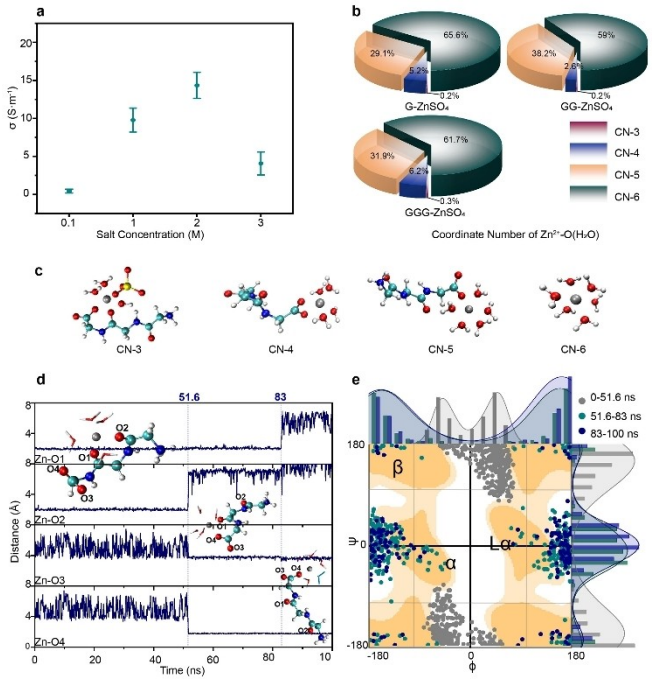

Figure 4. a) Electrical conductivities of electrolytes (with and without additives) at different concentrations. (Standard error of the mean is taken). **b)** Variation of Zn^{2+} CN distributions (3–6) in the 2 M $ZnSO_4$-0.1 M additive (G, GG, GGG) simulation system. **c)** Snapshots of Zn^{2+} coordination when the number of coordinated water molecules is 3, 4, 5, and 6. **d)** Variation of distances between Zn^{2+} and oxygen atoms (O1, O2, O3, O4 on the same triglycine) throughout the dynamical simulation, and snapshots of different oxygen atoms into the solvation sheath of Zn^{2+}. **e)** Distribution of φ and ψ dihedral angles over time on triglycine (triglycine in the example of Figure 4c).

simulation trajectory. During the 100.0 ns simulation process, we capture two ligand exchange events (Figure 4d), which undergo three metastable states lasting 51.6 ns, 31.4 ns, and 17.0 ns, respectively. For convenience in description, we label the four oxygen atoms on the triglycine as O1, O2, O3, and O4. From 0–51.6 ns, O1 and O2 are in the 1st solvation sheath of the Zn^{2+}, and the distance between the Zn^{2+} and O1 or O2 remains consistently at 2 Å, while the distance between O3, O4 and the Zn^{2+} fluctuates within the range of 4–7 Å. At 51.6 ns, O2 departed from the first hydration shell of Zn^{2+}, and the distance between them is stretched to approximately 7.0 Å. Then, O1 continues to occupy the coordination site of Zn^{2+}, while O4 rapidly enters the first hydration shell. Meanwhile, O3 begins to maintain a distance of 4 Å from Zn^{2+}, remaining within the second hydration shell. In the third process (83.0–100.0 ns), O4 and O3 maintain distances of 2 Å and 4 Å from the Zn^{2+}, respectively, residing within the first and second hydration shells, while O1 drops out the hydration shell. This process demonstrates the dynamic sliding capability of Zn^{2+} among multiple coordination sites of GGG. Even when some oxygen atoms detach from the hydration sheath, other oxygen atoms can quickly substitute for them, inhibiting the entry of active water molecules. This dynamic coordination adjustment mechanism reveals the stabilizing coordination effect of GGG on Zn^{2+}.

The dynamic sliding mechanism allows for efficient movement of Zn^{2+} ions along the GGG main chain. This enhanced mobility is also critical for improving the rate capability of zinc batteries, as it facilitates faster ion transport during charging and discharging processes. This can lead to higher power densities and reduced charging times. Unlike static binding sites, the dynamic nature of the sliding mechanism minimizes the risk of ion trapping within the electrolyte matrix. Ion trapping is a common issue in many battery systems, leading to reduced capacity and efficiency over time. By enabling continuous ion movement, the sliding mechanism helps maintain a consistent ionic conductivity, thereby enhancing the overall performance and longevity of the battery. The dynamic interaction between Zn^{2+} ions and the triglycine main chain provides a flexible environment that can adapt to the changing electrochemical conditions during battery operation. This adaptability helps in mitigating the formation of dendrites and other undesirable side reactions, which are common challenges in zinc-based batteries. As a result, the battery exhibits better cycling stability and a longer operational lifespan.

To demonstrate the dynamic conformational changes of GGG during the migration of Zn^{2+} between the active sites, we conduct a detailed analysis by calculating the temporal evolution of the dihedral angles φ and[56] of the GGG, subsequently plotting the Ramachandran map (Figure 4e). The results show that GGG adopts distinct conformational orientations at different stages of the migration process. The orange and light orange areas in the Figure 4e delineate the predominant conformational distribution of GGG in aqueous solution, with the white areas signifying rare conformations. For comparison, we also carry out MD simulations of the pure triglycine aqueous solution system and plot the evolution of the triglycine φ and ψ angles in this system (Figure S9). These comparative results indicate that the distributions of φ and ψ angles are usually concentrated within the following ranges: $-73° < \psi < 72.5°$, $-179° < \varphi < -110°$, $-66° < \psi < 60°$, and $113° < \varphi < 179°$. However, in the presence of Zn^{2+} in proximity to GGG, the angular distribution appears anomalous, with the ranges shifting to $78° < \psi < 179°$, $-54° < \varphi < 60°$, $-179° < \psi < 71°$, and $-72° < \varphi < 52°$. These observations underscore the significant influence of Zn^{2+} on the conformational landscape of GGG, highlighting the complex interplay between the additive and the metal ion in the electrolytic environment.

Especially in the phase from 0–51.6 ns, the Zn^{2+} first coordinates with O1 and O2, causing the initial conformation of GGG chain to be disrupted and the chain segments to be twisted, giving a rare conformation. This is due to the fact that O1 and O2 are located in the middle region of the chain and are separated by four atoms, which is a relatively long distance, and this coordination relationship limits the stretching of the chain segments. As Zn^{2+} gradually migrates to the C-terminal end of the GGG short peptide chain and coordinates with the oxygen atom at the C-terminal end, the conformation of the chain begins to stretch gradually. This is because the two oxygen atoms at the carboxylic group are closer together, especially the position of the terminal O4 atom is more favorable for chain straightening. In the final stage, Zn^{2+}

Research Article
doi.org/10.1002/batt.202400735
Chemistry Europe
European Chemical Societies Publishing

coordinates only with O4 at the carbonyl group, prompting a complete stretching of GGG in a conformation similar to the angular distribution without the intervention of Zn^{2+}. In addition, the appearance of GGG in α, β, and Lα conformations are observed. It is evident that the interaction between Zn^{2+} and the active sites in the GGG molecule alters the internal interactions and spatial arrangement of the GGG molecules, thereby affecting the distribution of their φ and ψ angles. In other words, the preferred conformation of GGG can be adjusted to accommodate coordination with Zn^{2+}. This conformational change may lead to a transition of the GGG molecule from a low-energy stable conformation to a higher-energy transition state or unstable state, ultimately impacting its overall dynamic behavior.

Thermodynamic Analysis

To probe more deeply into the physicochemical mechanism by which the oligopeptide additive enters the solvation sheath of Zn^{2+} and thus modifies the environment surrounding Zn^{2+}, we calculate the interaction energies between the water molecules, three kinds of additives, and Zn^{2+} by using density-functional theory (DFT). As shown in Figure S10, the binding energies of Zn^{2+} with G, GG and GGG are −31.1 kcal/mol, −40.9 kcal/mol, and −42.7 kcal/mol, respectively. The binding energies between Zn^{2+} and additives are significantly stronger than that between Zn^{2+} and water molecules (−16.8 kcal/mol), suggesting that oligopeptide molecule exhibit stronger interactions when bound to Zn^{2+}, especially GGG. This is consistent with the calculation of the Zn^{2+} with CN in Figure 4b, where GGG is more likely to displace water and thus bind directly to Zn^{2+}. This preferential adsorption reduces the probability of direct contact between water molecules and Zn^{2+}, and the additive is able to optimize the solvated structure of Zn^{2+} by being stably located around them in the electrolyte environment.

From the perspective of frontier molecular orbital theory, the energy gaps between the highest occupied molecular orbital (HOMO) and the lowest unoccupied molecular orbital (LUMO) for GGG, GG, and G are determined to be 10.0 eV, 8.6 eV, and 8.4 eV, respectively. These values are considerably lower than that observed for water molecules, which is 12.7 eV (Figure S11). This disparity suggests that glycine-based molecules are more readily excited and can preferentially adsorb onto the surface of zinc electrodes, thereby occluding the native hydrogen evolution sites and effectively mitigating hydrogen generation.[57] This observation underscores the efficacy of glycine as a side-reaction inhibitor in the deposition process of zinc electrodes, which can substantially enhance the stability and deposition efficiency of these electrodes.[27] Given that desolvation is often considered the rate-limiting step in metal deposition processes, the reduction of the desolvation energy barrier is instrumental in improving the stability of Zn^{2+} deposition and exfoliation.[58,59] The introduction of glycine as an additive, therefore, not only ameliorates the performance of the electrodes but also presents a novel avenue for optimizing the deposition processes of zinc electrodes.

The interaction energies of the formation of solvated structures during the stepwise desolvation of the [GGG-Zn^{2+}-$(H_2O)_5$] complexes are −118.0, 102.5, −95.7, −77.8, −62.8, −42.7 kcal/mol, [GG-Zn^{2+}-$(H_2O)_5$]−−131.7, 109.4, −94.0, −76.7, −61.2, −40.9 kcal/mol, while [G-Zn^{2+}-$(H_2O)_5$] structures formed during the desolvation of the complexes are −117.1, 100.7, −82.9, −71.7, −52.5, and −31.1 kcal/mol, respectively. These values are lower than those observed for the [Zn^{2+}-$(H_2O)_5$] complexes of (−106.4, −86.7, −70.2, −53.2, −37.9, −16.8 kcal/mol), indicating that the solvated structures formed with the participation of two additive molecules are more thermodynamically stable. The stepwise desolvation energies of the [GGG-Zn^{2+}-$(H_2O)_5$], [GG-Zn^{2+}-$(H_2O)_5$] and [G-Zn^{2+}-$(H_2O)_5$] complexes roughly show a lower energy barrier than that of [Zn^{2+} $(H_2O)_6$] (shown in Figure 5a, Figure S12, and Table S3). Fluctuations in energy barriers, characterized by abrupt decreases or increases, are observed in certain desolvation steps, potentially attributable to the high number of polar groups and atoms present on the molecules of the two glycine additives. Despite these variations, the total desolvation energy barrier post-additive introduction remains significantly lower than that of the system devoid of additives, with the solvated structure involving GGG being particularly noteworthy. The process of replacing a coordinated water molecule with G and GGG is as follows: $[Zn^{2+}(H_2O)_6] + G \rightarrow [G\text{-}Zn^{2+}(H_2O)_5] + H_2O$, $[Zn^{2+}(H_2O)_6] + GGG \rightarrow [GGG\text{-}Zn^{2+}(H_2O)_5] + H_2O$. The free energy changes for these processes are 10.7 kcal/mol and 11.7 kcal/mol, respectively, aligning with the results obtained from metaD simula-

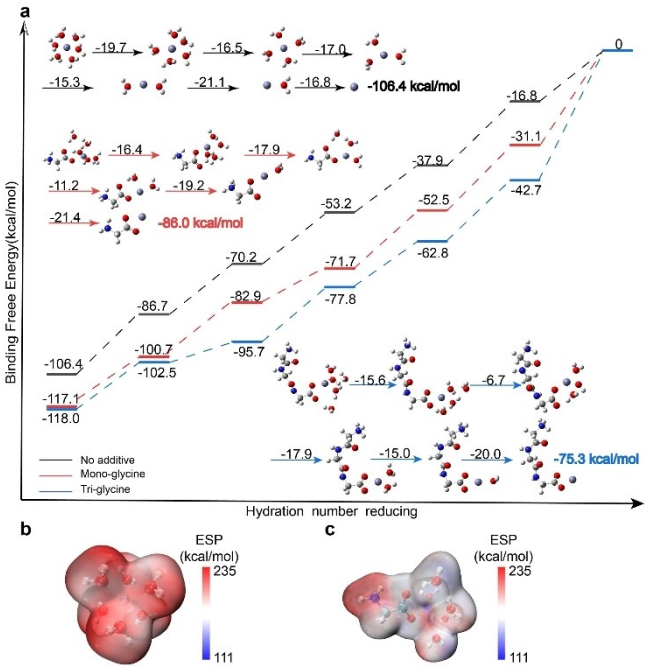

Figure 5. a) Energy changes during the desolvation process of [$Zn^{2+}(H_2O)_6$], [GGG-$Zn^{2+}(H_2O)_5$] and [G-$Zn^{2+}(H_2O)_5$] are computed, with corresponding structural models developed. [$Zn^{2+}(H_2O)_6$], [G-Zn^{2+}-$(H_2O)_5$] and [GGG-Zn^{2+}-$(H_2O)_5$] desolvation energy barriers during the stepwise desolvation process and the total desolvation energy barrier. **b–c)** The electrostatic potential maps of the solvated structures: [$Zn^{2+}(H_2O)_6$] and [G-$Zn^{2+}(H_2O)_5$] with their structural models.

tions. In addition, the introduction of a glycine in place of a water molecule in the original $[Zn^{2+}(H_2O)_6]$ structure resulted in a significant decrease in the electrostatic potential values (Figure 5b–c). This reinforces the observation that Zn^{2+} ions exhibit a heightened propensity to complex with GGG, thereby forming a novel solvation structure that is thermodynamically favorable.

Eelectrochemical tests can further validate the improvement in battery performance brought by the introduction of glycine additives. In the prior experiments, Yang et al.[33] analyzed the deposition behavior of Zn^{2+} on zinc electrodes under an overpotential of −150 mV using chronoamperometry (CA) curves, confirming that the ZS/GGG electrolyte promotes the formation of a uniform zinc deposition layer. Additionally, Song et al.[60] found that glycine molecules preferentially adsorb on the surface of the zinc anode, altering the interface between the zinc anode and the electrolyte. This increases the nucleation overpotential and inhibits the 2D diffusion of Zn^{2+}, thereby facilitating homogeneous zinc deposition.

Conclusions

In conclusion, we select glycine and its oligomers (GG, GGG, GGGG) as $ZnSO_4$ electrolyte additives to elucidate the dynamic mechanism by which these additives refine the coordination environment of Zn^{2+}. Through metadynamics simulations, we find that the energies for mono-, di-, tri- and tetraglycine to replace a water molecule in the 1st solvation sheath of the Zn^{2+} are 8.2 kcal/mol, 8.7 kcal/mol, 7.3 and 7.2 kcal/mol, respectively, indicating a slightly higher energy barrier. This reasonably explains the anomalous phenomenon we observe, in which additive molecules readily replace sulfate ions to enter the hydration layer of Zn^{2+}, rather than displacing water molecules. Additionally, we observe that as the number of binding sites on the additive molecules increases, Zn^{2+} can slide along the additive body; furthermore, the preferred conformation of GGG is disrupted to allow for direct coordination with Zn^{2+}. Further quantitative calculations reveal that the electrostatic interactions are the predominant force between additives and Zn^{2+} predominate. In 2 M $ZnSO_4$ electrolyte solution as the optimal conductivity, the interaction energy between GGG and Zn^{2+} is −214.5 kcal/mol, in contrast to the −16.8 kcal/mol observed between Zn^{2+} and water. The total desolvation energy barrier for the new solvation structure $[GGG\text{-}Zn^{2+}\text{-}(H_2O)_5]$ formed by triglycine is −75.3 kcal/mol, whereas it is −106.4 kcal/mol for $[Zn^{2+}(H_2O)_6]$. This significantly reduced desolvation energy barrier is instrumental in hastening the release of solvent molecules, thereby enhancing the interfacial ion diffusion rate and optimizing the deposition process. Collectively, these findings furnish a substantive foundation for the optimization of electrolyte solutions through the incorporation of glycine-based additives and present novel avenues for the enhancement of zinc anode performance.

Moreover, Coulombic efficiency (CE) is an important parameter for evaluating battery lifespan. Experimental work by Song et al.[60] confirmed that the CE of zinc-ion batteries with the addition of monoglycine reached 98.4%. Similarly, Yang et al.[33] found that the CE of the first cycle increased from 73.4%–87.51% after the introduction of the GGG molecule. These results demonstrate that glycine-based additives can significantly optimize the CE and overall performance of AZIBs, improving their stability and longevity. Collectively, these findings furnish a substantive foundation for the optimization of electrolyte solutions through the incorporation of glycine-based additives and present novel avenues for the enhancement of zinc anode performance.

Acknowledgements

This work was supported by National Natural Science Foundation of China (22203032). X.H. was supported by the National Natural Science Foundation of China (Grant Nos. 92477103 and 22273023), the National Key R&D Program of China (Grant No. 2019YFA0905200), Shanghai Municipal Natural Science Foundation (Grant No. 23ZR1418200), the Natural Science Foundation of Chongqing, China (Grant No. CSTB2023NSCQ-MSX0616), the Shanghai Frontiers Science Center of Molecule Intelligent Syntheses, Shanghai Future Discipline Program (Quantum Science and Technology), Shanghai Municipal Education Commission's "Artificial Intelligence-Driven Research Paradigm Reform and Discipline Advancement Program" and the Fundamental Research Funds for the Central Universities. We also thank the Supercomputer Center of East China Normal University (ECNU Multifunctional Platform for Innovation 001) for providing computer resources.

Conflict of Interests

The authors declare no conflict of interest.

Data Availability Statement

The data that support the findings of this study are available from the corresponding author upon reasonable request.

Keywords: Aqueous zinc-ion batteries · Additives · Glycine · Solvation structure

[1] J. H. Huang, Z. W. Guo, Y. Y. Ma, D. Bin, Y. G. Wang, Y. Y. Xia, *Small Methods* **2019**, *3*, 1800272.
[2] A. Konarov, N. Voronina, J. H. Jo, Z. Bakenov, Y.-K. Sun, S.-T. Myung, *ACS Energy Lett.* **2018**, *3*, 2620–2640.
[3] P. Ruan, S. Liang, B. Lu, H. J. Fan, J. Zhou, *Angew. Chem. Int. Ed.* **2022**, *61*, e202200598.
[4] H. Jia, Z. Q. Wang, B. Tawiah, Y. D. Wang, C.-Y. Chan, B. Fei, F. Pan, *Nano Energy* **2020**, *70*, 104523.
[5] L. E. Blanc, D. Kundu, L. F. Nazar, *Joule* **2020**, *4*, 771–799.
[6] Y. Y. Liu, X. Lu, F. L. Lai, T. X. Liu, P. R. Shearing, I. P. Parkin, G. He, D. J. L. Brett, *Joule* **2021**, *5*, 2845–2903.
[7] A. Chen, C. Y. Zhao, J. Z. Gao, Z. K. Guo, X. Y. Lu, J. C. Zhang, Z. P. Liu, M. Wang, N. N. Liu, L. S. Fan, Y. Zhang, N. Q. Zhang, *Energy Environ. Sci.* **2023**, *16*, 275–284.

[8] P. Xiao, H. B. Li, J. Z. Fu, C. Zeng, Y. H. Zhao, T. Y. Zhai, H. Q. Li, *Energy Environ. Sci.* **2022**, *15*, 1638–1646.
[9] J. N. Gu, Y. Tao, H. Chen, Z. J. Cao, Y. Z. Zhang, Z. G. Du, Y. L. S. Cui, S. B. Yang, *Adv. Energy Mater.* **2022**, *12*, 2200115.
[10] Y. Zong, H. W. He, Y. Z. Wang, M. H. Wu, X. C. Ren, Z. C. Bai, N. N. Wang, X. Ning, S. X. Dou, *Adv. Energy Mater.* **2023**, *13*, 2300403.
[11] L. Lin, S. L. Tian, Z. Y. Hu, Y. Zhang, L. M. Chang, J. J. Wang, W. Q. Liu, Q. S. Wang, F. Wang, *Chin. Chem. Lett.* **2024**, *35*, 109802.
[12] J. Guo, J. Y. Du, W. Q. Liu, G. Huang, X. B. Zhang, *Angew. Chem. Int. Ed.* **2024**, *63*, e202406465.
[13] Z. Y. Hu, L. Lin, Y. Jiang, L. S. Sun, W. Q. Liu, Q. S. Wang, F. Wang, *Energy Storage Mater.* **2024**, *73*, 103820.
[14] J. H. Cao, F. Zhao, W. X. Guan, X. X. Yang, Q. D. Zhao, L. G. Gao, X. F. Ren, G. Wu, A. M. Liu, *Small* **2024**, *20*, 2400221.
[15] F. Wan, L. L. Zhang, X. Dai, X. Y. Wang, Z. Q. Niu, J. Chen, *Nat. Commun.* **2018**, *9*, 1656.
[16] Z. Liu, T. Cui, G. Pulletikurthi, A. Lahiri, T. Carstens, M. Olschewski, F. Endres, *Angew. Chem. Int. Ed.* **2016**, *55*, 2889–2893.
[17] G.-M. Weng, Z. J. Li, G. T. Cong, Y. C. Zhou, Y.-C. Lu, *Energy Environ. Sci.* **2017**, *10*, 735–741.
[18] S. Guo, L. P. Qin, T. S. Zhang, M. Zhou, J. Zhou, G. Z. Fang, S. Q. Liang, *Energy Storage Mater.* **2021**, *34*, 545–562.
[19] Y. F. Geng, L. Pan, Z. Y. Peng, Z. F. Sun, H. C. Lin, C. W. Mao, L. Wang, L. Dai, H. D. Liu, K. M. Pan, X. W. Wu, Q. B. Zhang, Z. X. He, *Energy Storage Mater.* **2022**, *51*, 733–755.
[20] Y. H. Dai, C. Y. Zhang, W. Zhang, L. M. Cui, C. M. Ye, X. F. Hong, J. H. Li, R. W. Chen, W. Zong, X. Gao, J. X. Zhu, P. E. Jiang, Q. Y. An, D. J. L. Brett, I. P. Parkin, G. J. He, L. Q. Mai, *Angew. Chem. Int. Ed.* **2023**, *62*, e202301192.
[21] M. Kim, S.-J. Shin, J. Lee, Y. Park, Y. Kim, H. Kim, J. W. Choi, *Angew. Chem. Int. Ed.* **2022**, *61*, e202211589.
[22] Y. P. Zhu, J. Yin, X. L. Zheng, A.-H. Emwas, Y. J. Lei, O. F. Mohammed, Y. Cui, H. N. Alshareef, *Energy Environ. Sci.* **2021**, *14*, 4463–4473.
[23] Q. Zhang, J. Y. Luan, L. Fu, S. A. Wu, Y. G. Tang, X. B. Ji, H. Y. Wang, *Angew. Chem. Int. Ed.* **2019**, *58*, 15841–15847.
[24] K. E. K. Sun, T. K. A. Hoang, T. N. L. Doan, Y. Yu, X. Zhu, Y. Tian, P. Chen, *ACS Appl. Mater. Interfaces* **2017**, *9*, 9681–9687.
[25] H. J. Huang, J. W. Yun, H. Feng, T. Tian, J. W. Xu, D. L. Li, X. Xia, Z. H. Yang, W. X. Zhang, *Energy Storage Mater.* **2023**, *55*, 857–866.
[26] J. Xu, W. L. Lv, W. Yang, Y. Jin, Q. Z. Jin, B. Sun, Z. L. Zhang, T. Y. Wang, L. F. Zheng, X. L. Shi, B. Sun, G. X. Wang, *ACS Nano* **2022**, *16*, 11392–11404.
[27] Z. Y. Jiao, X. X. Cai, X. X. Wang, Y. R. Li, Z. Bie, W. X. Song, *Adv. Energy Mater.* **2023**, *13*, 2302676.
[28] Z. G. Hou, M. F. Dong, Y. L. Xiong, X. Q. Zhang, H. Ao, M. K. Liu, Y. C. Zhu, Y. T. Qian, *Small* **2020**, *16*, 2001228.
[29] Q. Z. Gou, H. R. Luo, Q. Zhang, J. B. Deng, R. Z. Zhao, O. Odunmbaku, L. Wang, L. J. Li, Y. J. Zheng, J. Li, D. L. Chao, M. Li, *Small* **2023**, *19*, 2207502.
[30] C. Y. Lin, L. J. He, P. X. Xiong, H. Lin, W. B. Lai, X. H. Yang, F. Y. Xiao, X.-L. Sun, Q. R. Qian, S. D. Liu, Q. H. Chen, S. Kaskel, L. X. Zeng, *ACS Nano* **2023**, *17*, 23181–23193.
[31] Z. Luo, Y. F. Xia, S. Chen, X. X. Wu, R. Zeng, X. Zhang, H. G. Pan, M. Yan, T. T. Shi, K. Tao, B. B. Xu, Y. Z. Jiang, *Nano-Micro Lett.* **2023**, *15*, 205.
[32] Y. Liu, Y. K. An, L. Wu, J. G. Sun, F. Y. Xiong, H. Tang, S. L. Chen, Y. Guo, L. Zhang, Q. Y. An, L. Q. Mai, *ACS Nano* **2023**, *17*, 552–560.
[33] J. Zhang, Y. X. Liu, Y. J. Wang, Z. J. Zhu, Z. L. Yang, *Adv. Funct. Mater.* **2024**, *34*, 2401889.
[34] M. J. Abraham, T. Murtola, R. Schulz, S. Páll, J. C. Smith, B. Hess, E. Lindahl, *SoftwareX* **2015**, *1–2*, 19–25.
[35] T. Lu, *Sobtop* **n.d.**, *Version 1.0(dev3.2)*, DOI http://sobereva.com/soft/Sobtop (accessed on 09/25/2024).
[36] C. D. Williams, P. Carbone, *J. Chem. Phys.* **2015**, *143*, 174502.
[37] H. J. C. Berendsen, J. R. Grigera, T. P. Straatsma, *J. Phys. Chem.* **1987**, *91*, 6269–6271.
[38] M. Bonomi, D. Branduardi, G. Bussi, C. Camilloni, D. Provasi, P. Raiteri, D. Donadio, F. Marinelli, F. Pietrucci, R. A. Broglia, M. Parrinello, *Comput. Phys. Commun.* **2009**, *180*, 1961–1972.
[39] G. A. Tribello, M. Bonomi, D. Branduardi, C. Camilloni, G. Bussi, *Comput. Phys. Commun.* **2014**, *185*, 604–613.
[40] M. Bonomi, G. Bussi, C. Camilloni, G. A. Tribello, P. Banáš, A. Barducci, M. Bernetti, P. G. Bolhuis, S. Bottaro, D. Branduardi, R. Capelli, P. Carloni, M. Ceriotti, A. Cesari, H. Chen, W. Chen, F. Colizzi, S. De, M. De La Pierre, D. Donadio, V. Drobot, B. Ensing, A. L. Ferguson, M. Filizola, J. S. Fraser, H. Fu, P. Gasparotto, F. L. Gervasio, F. Giberti, A. Gil-Ley, T. Giorgino, G. T. Heller, G. M. Hocky, M. Iannuzzi, M. Invernizzi, K. E. Jelfs, A. Jussupow, E. Kirilin, A. Laio, V. Limongelli, K. Lindorff-Larsen, T. Löhr, F. Marinelli, L. Martin-Samos, M. Masetti, R. Meyer, A. Michaelides, C. Molteni, T. Morishita, M. Nava, C. Paissoni, E. Papaleo, M. Parrinello, J. Pfaendtner, P. Piaggi, G. Piccini, A. Pietropaolo, F. Pietrucci, S. Pipolo, D. Provasi, D. Quigley, P. Raiteri, S. Raniolo, J. Rydzewski, M. Salvalaglio, G. C. Sosso, V. Spiwok, J. Šponer, D. W. H. Swenson, P. Tiwary, O. Valsson, M. Vendruscolo, G. A. Voth, A. White, *Nat. Methods* **2019**, *16*, 670–673.
[41] B. Hess, H. Bekker, H. J. C. Berendsen, J. G. E. M. Fraaije, *J. Comput. Chem.* **1997**, *18*, 1463–1472.
[42] G. Bussi, D. Donadio, M. Parrinello, *J. Chem. Phys.* **2007**, *126*, 014101.
[43] M. J. Frisch, G. W. Trucks, H. B. Schlegel, G. E. Scuseria, M. A. Robb, J. R. Cheeseman, G. Scalmani, V. Barone, G. A. Petersson, H. Nakatsuji, X. Li, M. Caricato, A. V. Marenich, J. Bloino, B. G. Janesko, R. Gomperts, B. Mennucci, H. P. Hratchian, J. V. Ortiz, A. F. Izmaylov, J. L. Sonnenberg, F.WilliamsDingDing, F. Lipparini, F. Egidi, J. Goings, B. Peng, A. Petrone, T. Henderson, D. Ranasinghe, V. G. Zakrzewski, J. Gao, N. Rega, G. Zheng, W. Liang, M. Hada, M. Ehara, K. Toyota, R. Fukuda, J. Hasegawa, M. Ishida, T. Nakajima, Y. Honda, O. Kitao, H. Nakai, T. Vreven, K. Throssell, J. A. Montgomery Jr., J. E. Peralta, F. Ogliaro, M. J. Bearpark, J. J. Heyd, E. N. Brothers, K. N. Kudin, V. N. Staroverov, T. A. Keith, R. Kobayashi, J. Normand, K. Raghavachari, A. P. Rendell, J. C. Burant, S. S. Iyengar, J. Tomasi, M. Cossi, J. M. Millam, M. Klene, C. Adamo, R. Cammi, J. W. Ochterski, R. L. Martin, K. Morokuma, O. Farkas, J. B. Foresman, D. J. Fox, **2016**.
[44] K.-M. Tu, R. Ishizuka, N. Matubayasi, *J. Chem. Phys.* **2014**, *141*, 044126.
[45] J.-P. Hansen, I. R. McDonald, *Theory of Simple Liquids With Applications to Soft Matter* **2013**.
[46] T. Lu, F. W. Chen, *J. Comput. Chem.* **2012**, *33*, 580–592.
[47] W. Humphrey, A. Dalke, K. Schulten, *J. Mol. Graph.* **1996**, *14*(33–38), 27–28.
[48] D. D. Feng, Y. C. Jiao, P. Y. Wu, *Angew. Chem. Int. Ed.* **2023**, *62*, e202215060.
[49] R. W. Chen, W. Zhang, Q. B. Huang, C. H. Guan, W. Zong, Y. H. Dai, Z. J. Du, Z. Y. Zhang, J. W. Li, F. Guo, X. Gao, H. B. Dong, J. X. Zhu, X. H. Wang, G. J. He, *Nano-Micro Lett.* **2023**, *15*, 81.
[50] X. Y. Yu, M. Chen, Z. G. Li, X. Tan, H. T. Zhang, J. H. Wang, Y. L. Tang, J. P. Xu, W. Yin, Y. Yang, D. L. Chao, F. Wang, Y. G. Zou, G. Feng, Y. Qiao, H. S. Zhou, S.-G. Sun, *J. Am. Chem. Soc.* **2024**, *146*, 17103–17113.
[51] K. Lu, C. L. Chen, Y. Wu, C. Liu, J. J. Song, H. Y. Jing, P. Zhao, B. Y. Liu, M. Z. Xia, Q. L. Hao, W. Lei, *Chem. Eng. J.* **2023**, *457*, 141287.
[52] X. Cheng Liang, X. F. Chen, Z. Xiang Zhai, R. S. Huang, T. Q. Yu, S. B. Yin, *Chem. Eng. J.* **2024**, *480*, 148040.
[53] F. F. Wu, Y. C. Chen, Y. L. Chen, R. L. Yin, Y. C. Feng, D. Zheng, X. L. Xu, W. H. Shi, W. X. Liu, X. H. Cao, *Small* **2022**, *18*, 2202363.
[54] D. D. Feng, F. Q. Cao, L. Hou, T. Y. Li, Y. C. Jiao, P. Y. Wu, *Small* **2021**, *17*, 2103195.
[55] J. T. Hinatsu, V. D. Tran, F. R. Foulkes, *J. Appl. Electrochem.* **1992**, *22*, 215–223.
[56] R. A. Laskowsk, M. W. Macarthu, D. S. Moss, J. M. Thornton, *J. Appl. Crystallogr.* **1993**, 283–291.
[57] Q. Zhang, Y. L. Ma, Y. Lu, Y. X. Ni, L. Lin, Z. K. Hao, Z. H. Yan, Q. Zhao, J. Chen, *J. Am. Chem. Soc.* **2022**, *144*, 18435–18443.
[58] A. Gupta, A. Manthiram, *Adv. Energy Mater.* **2020**, *10*, 2001972.
[59] T. Ma, Y. X. Ni, Q. R. Wang, W. J. Zhang, S. Jin, S. B. Zheng, X. Yang, Y. P. Hou, Z. L. Tao, J. Chen, *Angew. Chem. Int. Ed.* **2022**, *61*, e202207927.
[60] Z. H. Guo, X. Y. Mo, Y. Xu, X. N. Xu, L. L. Shi, H. R. Wan, L. M. Sun, W. C. Zhuang, M. Song, *J. Electron. Mater.* **2024**, *53*, 6594–6604.

Manuscript received: November 14, 2024
Revised manuscript received: January 26, 2025
Accepted manuscript online: February 13, 2025
Version of record online: February 25, 2025